Multistep effects in the elastic and inelastic scattering of 70.4-MeV ^{12}C ions from the even neodymium isotopes

D. L. Hillis,* E. E. Gross, and D. C. Hensley
Oak Ridge National Laboratory, † Oak Ridge, Tennessee 37830

C. R. Bingham
University of Tennessee, ‡ Knoxville, Tennessee 37916

F. T. Baker and A. Scott
University of Georgia, § Athens, Georgia 30601

(Received 6 July 1977)

The interference of Coulomb and nuclear excitation was studied by the scattering of 70.4-MeV ^{12}C ions from the stable even Nd nuclei (^{142}Nd, ^{144}Nd, ^{146}Nd, ^{148}Nd, ^{150}Nd). The differential cross sections for inelastic scattering from the low-lying 2^+, 4^+, 3^-, and 2_2^+ states, as well as elastic scattering from these isotopes, were obtained. In addition, the cross sections for exciting the 2^+ (4.43 MeV) state of the ^{12}C projectile and the 6^+ state in ^{150}Nd were also obtained. The differential cross sections for exciting low-lying collective states of the target and projectile are compared with distorted-wave Born-approximation and coupled-channels calculations. Standard distorted-wave Born-approximation calculations using known Coulomb matrix elements fail to fit the data. The coupled-channels analysis, however, can account for these data and reveals the importance of multistep processes in heavy ion reactions.

[NUCLEAR REACTIONS $^{142,144,146,148,150}Nd(^{12}C, ^{12}C)$, $(^{12}C, ^{12}C')$, $E=70.4$ MeV; measured $\sigma(\theta)$. Deduced optical-model parameters in addition to β_2 and β_4 deformations by coupled-channel analyses. Enriched targets.]

I. INTRODUCTION

The determination of nuclear matter and charge distributions has long been an important stimulus to the development of both nuclear structure and nuclear reaction theories. Information on the moments of the nuclear charge distribution comes from analyses of experiments involving electromagnetic probes (e.g., electron scattering, Coulomb excitation, muon atomic transitions, etc.), whereas the primary source of information on nuclear matter distributions comes from analyses of hadronic scattering experiments. From the near perfect charge independence of nuclear forces, it is expected that nuclear matter and charge distributions should agree to about 1%.

The known analytic nature of the Coulomb interaction simplifies the extraction of nuclear structure information from electromagnetic measurements. On the other hand, analysis of hadronic scattering experiments must proceed by first determining a phenomenological interaction potential to represent the nuclear force. The nonunique nature of the optical model together with the usual uncertainties in the absolute value of light-ion cross sections (10–20%) have limited the reliability of deformation parameters obtained from light-ion scattering experiments. Within these limitations, there has been general agreement between Coulomb-excitation $B(E2)$ matrix elements and quadrupole deformation parameters (β_2) determined from distorted-wave Born-approximation (DWBA) analysis of light-ion inelastic scattering provided that geometrical factors are properly applied.[1]

The availability of high-energy heavy-ion beams has expanded the horizons for inelastic excitation by hadrons. Differential cross sections for energies slightly above the Coulomb barrier display interesting interference effects between Coulomb and nuclear excitation,[2] and the absolute normalization of the cross sections can be obtained with high accuracy by comparing with Rutherford scattering at forward angles. However, even with a proper treatment of the Hendrie scaling factors for the nuclear interaction,[1] the DWBA analysis for quadrupole excitations by heavy-ion inelastic scattering has required that nuclear deformation parameters be considerably smaller than Coulomb deformation parameters.[3-6] This failure of the single-step DWBA method has been attributed to strong two-step processes such as quadrupole reorientation in the case of 2^+ state excitation[7-9] and double $E2$ transitions in the case of 4^+ state excitation.[8] Proper treatment of multistep processes by the coupled-channels method[10] (CC) has revealed that heavy-ion inelastic scattering is quite sensitive to quadrupole moments of excited states

if the bombarding energy is above the Coulomb barrier.[7-9] To explore such effects further, we report herein experimental results and analysis of 70.4-MeV ^{12}C scattering on five even Nd isotopes. These isotopes span a deformation region from near spherical (^{142}Nd with $\beta_2 \simeq 0.10$) to very deformed (^{150}Nd with $\beta_2 \simeq 0.3$). Thus the Nd nuclei offer an excellent opportunity to study Coulomb-nuclear interference effects as a function of nuclear shape. In addition, the static quadrupole moments for the low-lying 2^+ states are large and increase steadily from ^{144}Nd ($Q_2 = -0.39$ *e* b) to ^{150}Nd ($Q_2 = -2.00$ *e* b).[11] The sensitivity of heavy-ion inelastic scattering to static quadrupole moments can consequently be systematically investigated.

II. EXPERIMENTAL DETAILS

The 70.4-MeV $^{12}C^{3+}$ ion beam was provided by the Oak Ridge isochronous cyclotron (ORIC). The extracted beam was magnetically analyzed to determine the beam energy[12] and then guided by a number of quadrupole magnetic lenses onto a target located at the center of a scattering chamber. An overall uncertainty of ±140 keV should be placed upon the beam energy determination of 70.4 MeV.

Targets of ^{142}Nd, ^{144}Nd, ^{146}Nd, ^{148}Nd, and ^{150}Nd were made by vacuum evaporation of enriched rare earth oxides onto 40-$\mu g/cm^2$ carbon backings. The oxide powders were obtained from the Separated Isotopes Division of the Oak Ridge National Laboratory, and the enrichments were 98.26% for ^{142}Nd, 97.51% for ^{144}Nd, 97.46% for ^{146}Nd, 95.44% for ^{148}Nd, and 96.13% for ^{150}Nd. Target thicknesses ranged from 140–180 $\mu g/cm^2$ as determined from the energy loss of 5.8-MeV α particles from a natural ^{244}Cm α source.

Angular distributions for elastic scattering on the various Nd targets were measured with a position-sensitive solid-state detector (PSD) located on one of the moveable arms of a 76-cm-diam scattering chamber. Beam wandering on the target was minimized by proper control of the quadrupole lenses and by positioning a slit system prior to the target. The beam preparation system was operated to limit the beam divergence to ±0.2° at the target and the absolute beam direction was determined to 0.1° by making detector measurements on both sides of the beam. A 15-aperture brass collimator was located immediately in front of the PSD. Each aperture was 0.50° wide, centered at 1.0° intervals, and one setting of the PSD spanned a range of 15°. This particular setup was used in the elastic scattering measurements for the ^{144}Nd and ^{146}Nd targets. The elastic scattering data on the ^{142}Nd, ^{148}Nd, and ^{150}Nd targets were acquired using a 25-aperture collimator with 0.60° openings centered at intervals of 0.63° which covered a range of 15.8°. The relative solid angles of the monitor detector and all apertures of the multislit array were determined to 1.5% accuracy by measuring α-particle yields from a ^{244}Cm source placed at the target position. The arm on which the 15-aperture PSD was mounted, was moved in 10° intervals to obtain complete angular distributions, and an overlap of five angles was measured each time. The 25-aperture detector was moved in 10.75° intervals to provide for an overlap of eight angles. The results from the overlapping regions of the angular distributions generally agreed within statistics. At the smallest angles studied, the finite height of the slits corresponded to an increase of $\leq 0.2°$ in the effective polar angle. Preliminary optical-model calculations for elastic scattering indicated that elastic scattering for $\theta_{c.m.} < 30°$ deviated from Rutherford scattering by less than 1%. Scattering at these angles was therefore used to absolutely normalize the data. We estimate the error on the absolute uncertainty to be 5%.

A conventional ΔE-E telescope was used on the left side of the beam to survey for possible contributions from reaction products to the energy region containing elastic events. The telescope consisted of Si surface barrier counters 70 μm thick for the ΔE element and 408 μm thick for the E element. From the telescope information it was deduced that no significant contributions from other nuclear reactions were present in our elastic scattering data. The overall energy resolution obtained for the elastic scattering measurements using the multislit arrangement was ~300 keV. This was insufficient to separate elastic scattering from the first 2^+ states of ^{148}Nd and ^{150}Nd. However, from the BRS data discussed below, we were able to separate these states and thereby correct for inelastic contamination. Further details on the experimental method and data reduction have been treated in more detail elsewhere.[13]

Inelastic scattering measurements were made using a Q1D magnetic spectrograph[14] with a position-sensitive gas proportional detector[15] at the focal plane. Care was taken to operate the beam preparation system and the BRS in a dispersion matching mode, to locate the focal plane, and to control other factors contributing to energy resolution. Factors related to target thickness and target nonuniformity appeared to limit the resolution to 115 keV. With this resolution, the lowest 2^+ state in ^{150}Nd appears as a shoulder on the low-energy side of the elastic peak. A sample ^{150}Nd spectrum is shown in Fig. 1(a). This spectrum was unfolded by using the elastic peak line

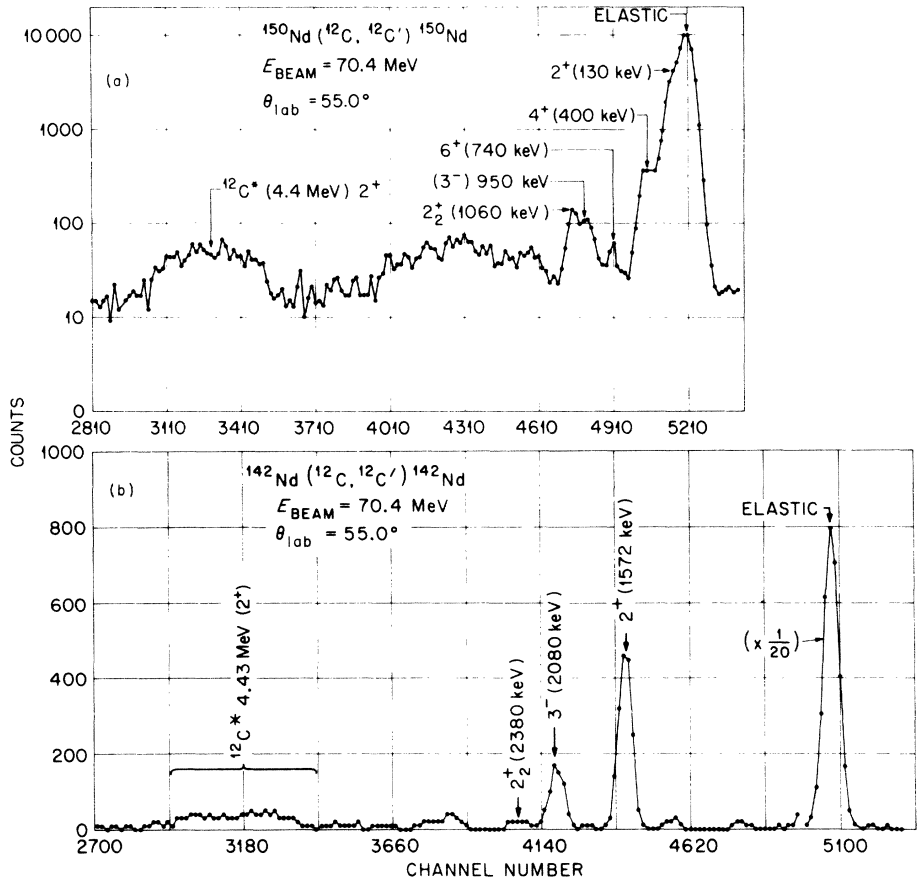

FIG. 1. Sample $^{12}C^{6+}$ spectra from the spectrograph measurements. Elastic peak line shapes from ^{142}Nd target measurements were used to unfold overlapping levels in ^{150}Nd target measurements.

shape from ^{142}Nd [Fig. 1(b)] taken at the same angle to represent the true peak shape in ^{150}Nd and ^{148}Nd. Treatment of the detector signals as well as the method of data reduction has been described previously.[16] The main innovation in this work was the addition of precision elastic scattering data described above, which were used to absolutely normalize the BRS data. Errors related to beam monitoring, target variations, solid angle variations, etc., which arise when normalizing BRS measurements at different angles were thereby eliminated. In this manner the absolute cross sections for exciting the low-lying 2$^+$, 4$^+$, 3$^-$, and 2^+_2 states in the even Nd isotopes were measured over the angular range $\sim 20° \leq \theta_{c.m.} \leq \sim 85°$. In addition, the absolute yields for the 6$^+$ state in ^{150}Nd and the 2$^+$ (4.43 MeV) state of the projectile ^{12}C were measured.

III. ELASTIC SCATTERING AND OPTICAL-MODEL ANALYSIS

The differential cross sections for 70.4-MeV ^{12}C elastic scattering from the five even Nd isotopes are shown in Fig. 2. They are plotted as ratios to Rutherford scattering on a linear scale to emphasize the oscillations before the exponential falloff near 50°. Statistical errors are smaller than the size of the data points. We note that the oscillations dampen with increasing mass or, more importantly, with increasing β_2 deformation. This effect had been noted previously with 12-MeV deuterons,[17] but it is much more pronounced with heavy-ion beams. A logarithmic plot would more easily reveal that the slopes of the exponential falloff are almost identical for ^{142}Nd, ^{144}Nd, and ^{146}Nd but become progressively steeper for ^{148}Nd and ^{150}Nd. These effects result from the removal of elastic flux by the excitation of highly collective states, especially the ground-state rotational band.

A conventional optical-model analysis using volume absorption of these data would search to find a set of real and imaginary geometry parameters (r_0, a_0, r', and a') common to all isotopes and attempt to account for cross section variations by varying the real and imaginary well depths (V and W). However, the variations from isotope to iso-

tope shown in Fig. 2 cannot be explained within the philosophy of the conventional optical model because of the strong coupled-channels effects alluded to above. Instead, the approach we took was to search for a common real potential (parameters V, r_0, and a_0) and to allow the imaginary potential (parameters W, r', and a') to account for variations from isotope to isotope. It was hoped that the subsequent coupled-channels analysis, with the collective states explicitly included in the calculation would reveal a common imaginary potential.[18] As we will see below, this hope was essentially realized and lends strong support for the coupled-channels (CC) approach.

We used a six parameter model which is described in detail in Ref. 13. Starting with the "shallow" potential for ^{12}C on ^{208}Pb from Ref. 13 and using the automatic search program GENOA,[19] we searched for a fit to each set of elastic scattering data in the following patterns: first search on V, r' and a'; then search on W, r_0, and a_0, and finally search on V and W. This strategy yielded the excellent fits shown as solid curves in Fig. 2.

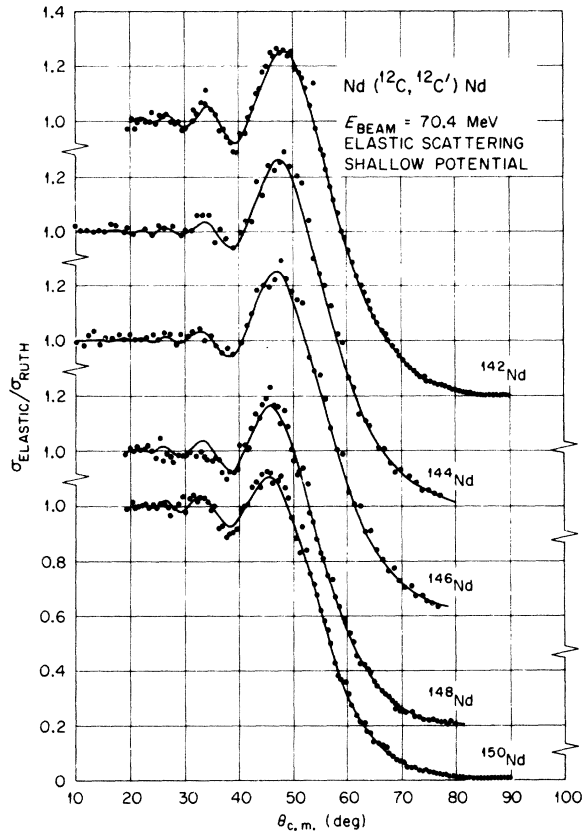

FIG. 2. Elastic scattering data for 70.4-MeV ^{12}C from the even Nd isotopes. The curves are optical-model calculations with the parameters from Table I or Table II.

TABLE I. Optical-model parameters providing the minimum χ^2 fits shown in Fig. 1.

	^{142}Nd	^{144}Nd	^{146}Nd	^{148}Nd	^{150}Nd
V (MeV)	15.07	17.15	18.18	30.24	25.04
r_0 (fm)	1.354	1.292	1.307	1.300	1.323
a_0 (fm)	0.481	0.691	0.640	0.522	0.474
W (MeV)	10.78	12.97	16.29	30.23	32.39
r' (fm)	1.335	1.334	1.353	1.108	1.015
a' (fm)	0.446	0.428	0.367	0.853	1.028
r_c (fm)	1.25	1.25	1.25	1.25	1.25
σ_r (b)	1.256	1.266	1.295	1.560	1.667
R_s (fm)	1.517	1.516	1.523	1.555	1.561
χ^2/N_p	1.5	1.3	3.3	1.8	1.9

The parameters, together with χ^2 per point, calculated total reaction cross sections σ_r, and strong absorption radii R_s are summarized in Table I. The strong absorption radius is defined by:

$$R_s = \frac{(\eta/k)}{(A_1^{1/3}+A_2^{1/3})}\left[1+\left(1+\frac{L(L+1)}{\eta^2}\right)^{1/2}\right], \qquad (1)$$

where L is the partial wave number for which the transmission coefficient is $\frac{1}{2}$, $\eta = Z_1 Z_2 e^2/\hbar v_{c.m.}$, k is the c.m. wave number, and A_1 and A_2 are the atomic masses of the projectile and target, respectively. We note that the total increase in R_s from ^{142}Nd to ^{150}Nd is larger than expected from an $A^{1/3}$ size variation. Again, because of the strong coupling to the collective excitations, it is not clear what significance can be placed on these apparent size variations. The strong coupling effect is also obvious from the increase in total reaction cross section σ_r, with increasing β_2 deformation of the target. These results should serve as a warning to the use of global optical-model parameters for estimating total reaction cross sections. From Table I, it is evident that if an optical-model representation for ^{142}Nd is used to estimate the total reaction cross section for 70-MeV ^{12}C incident on ^{150}Nd, the estimate would be low by 400 mb.

The parameters for the real well in Table I are

TABLE II. "Common real potential" optical-model parameters. The real potential parameters are $V = 20.0$ MeV, $r_0 = 1.315$ fm, and $a_0 = 0.562$ fm.

	^{142}Nd	^{144}Nd	^{146}Nd	^{148}Nd	^{150}Nd
W (MeV)	11.6	12.1	16.3	147.5	119.5
r' (fm)	1.341	1.341	1.341	1.007	1.040
a' (fm)	0.414	0.414	0.414	0.763	0.774
r_c (fm)	1.25	1.25	1.25	1.25	1.25
σ_r (b)	1.249	1.271	1.322	1.547	1.609
χ^2/N_p	1.9	1.6	3.4	1.8	2.8

similar for all five isotopes. A simple average together with additional searches yields the following "common real potential": $V = 20.0$ MeV, $r_0 = 1.315$ fm, and $a_0 = 0.562$ fm. With this potential fixed, we again searched on elastic scattering data, this time varying W, r', and a'. The resulting imaginary well parameters are summarized in Table II. Only for ^{150}Nd is there a significant increase in χ^2 relative to the best fits in Table I. These "common real geometry" fits are in fact indistinguishable from the best parameter fits shown in Fig. 2. It is this potential (with the appropriate imaginary part) that provided the starting point for the DWBA and CC analyses described below.

IV. INELASTIC SCATTERING–DWBA ANALYSIS

Figure 3 shows the states which were excited in the inelastic scattering of the 70.4-MeV ^{12}C ions from the various even Nd isotopes. The inelastic scattering data from each of the even Nd isotopes were first analyzed using the distorted-wave Born approximation (DWBA) with simple collective model form factors.[20] The DWBA code DWUCK[21] was used with 250 partial waves and an integration radius of 50 fm.

The spectroscopic results from the DWBA analysis of 2^+ and 3^- states are shown in Table III and are compared with previous results.[11,22–25] In all cases excellent fits to the data could be achieved but only by using quite different values of Coulomb and nuclear deformation lengths ($\beta_l R$). Representative fits are shown in Figs. 4 and 5. Also shown in these figures are the separate contributions of Coulomb and nuclear excitation. It is evident that the absence of a well-defined interference minimum in the 2^+ angular distribution (Fig. 4) is due to the dominance of Coulomb excitation in the region of "grazing" collisions ($\theta_{\text{c.m.}} \simeq 50°$). For the $l = 3$ transitions, however, Coulomb and nuclear excitation are comparable, and a well-defined interference minimum results (Fig. 5).

DWBA calculations for excitation of 4^+ states gave poor results regardless of the values of β_4^C and β_4^N. This is not surprising since multiple $l = 2$ excitations ($0^+ \rightarrow 2^+ \rightarrow 4^+$) are likely to be important. Coupled-channels analysis of the excitation of 4^+ states will be described in Sec. V B.

V. INELASTIC SCATTERING–COUPLED-CHANNELS ANALYSIS

The fact that the low-lying 2^+ and 3^- states were well described by DWBA calculations only if the nuclear deformation lengths were 35–50% smaller than the corresponding Coulomb deformation lengths is suggestive that the DWBA does not provide an adequate description of the reaction. Such large differences are not commonly found in light-ion scattering where the reaction mechanisms are generally better understood. In an earlier publication[8] we have shown, for ^{144}Nd, that this apparent inequality is removed when higher-order processes neglected in DWBA calculations, particularly reorientation, are included by performing coupled-channels calculations. Presented here is the systematic analysis of our survey of all even-A Nd isotopes; the success of this analysis, described below, for nuclei spanning the transition region from spherical to deformed, strongly supports this point of view.

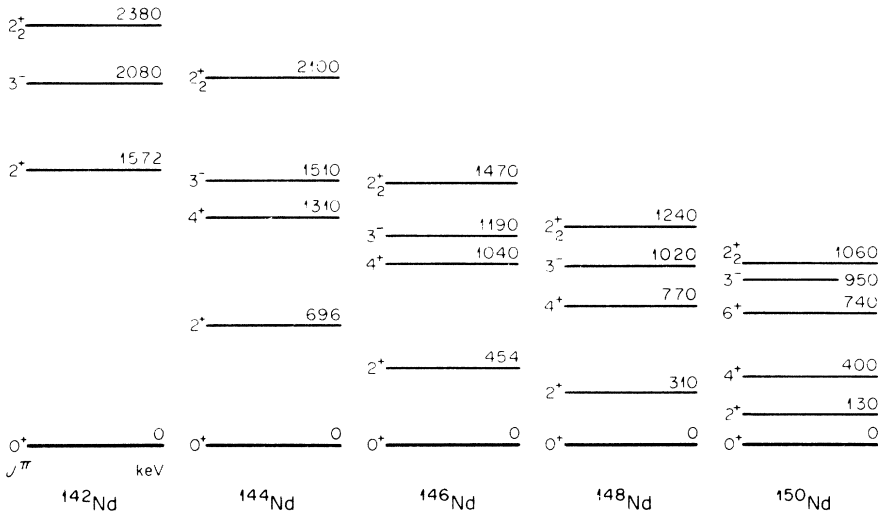

FIG. 3. The low-lying collective states of the even Nd isotopes which are strongly excited by 70.4-MeV ^{12}C inelastic scattering.

TABLE III. Deformation parameters deduced from the present DWBA analysis for the even Nd isotopes in comparison with the deformation parameters deduced from previous Coulomb excitation experiments.

		Previous Coulomb excitation					Present results			
Target	J^π	E^* (keV)	$B(El)\uparrow$ (e^2b^l)	$B(El)\uparrow$ [a] (spu)	β_l^C [c]	$\beta_l^C R_C$ [c] (fm)	β_l^C	β_l^N	$\beta_l^C R_C$ (fm)	$\beta_l^N R_N$ [b] (fm)
142	2^+	1572	0.34 [d]	15.6	0.104	0.65	0.10	0.06	0.64	0.42
	3^-	2080	0.24 [e]	28.6	0.139	0.87	0.14	0.08	0.88	0.57
144	2^+	696	0.40 [d]	18.0	0.111	0.70	0.12	0.08	0.75	0.54
	3^-	1510	0.26 [f]	30.2	0.143	0.90	0.16	0.10	1.01	0.68
146	2^+	454	0.76 [g]	33.5	0.152	0.96	0.16	0.10	1.01	0.69
	3^-	1190	0.24 [h]	27.1	0.136	0.86	0.18	0.10	1.14	0.69
148	2^+	310	1.36 [g]	58.9	0.202	1.28	0.21	0.14	1.33	0.96
	3^-	1020	...	...			0.15	0.11	0.95	0.76
150	2^+	130	2.65 [d]	112.7	0.279	1.78	0.32	0.20	2.04	1.41
	3^-	950	...	...			0.13	0.07	0.83	0.49

[a] For $B(E2)\uparrow$, 1 spu $= 2.95 \times 10^{-5} A_2^{4/3}\ e^2b^2$; for $B(E3)\uparrow$, 1 spu $= 4.158 \times 10^{-7} A_2^2\ e^2b^3$.
[b] $R_N = r_0 A_2^{1/3}$ and r_0 is given in Table I.
[c] β_l^C deduced from Eq. (2) with $R_C = 1.20 A_2^{1/3}$.
[d] See Ref. 22.
[e] See Ref. 23.
[f] See Ref. 25.
[g] See Ref. 11.
[h] See Ref. 24.

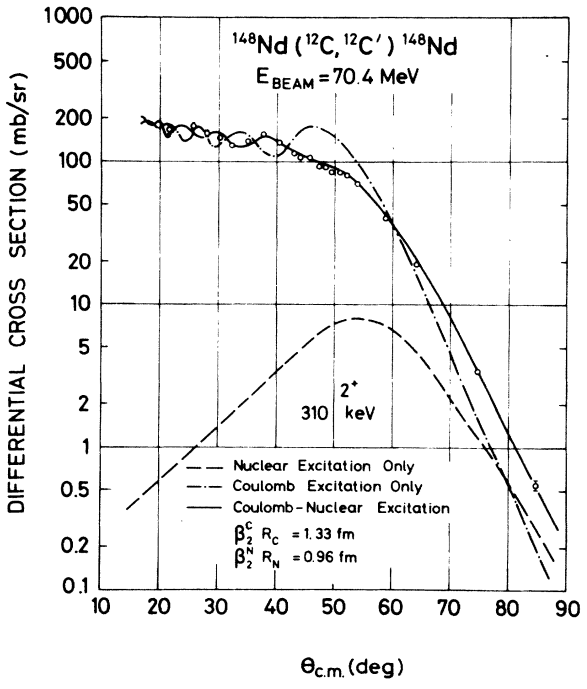

FIG. 4. Differential cross section for exciting the 2^+ (310-keV) state of ^{148}Nd by 70.4-MeV ^{12}C inelastic scattering. The solid curve is a DWBA fit to the data using the potential of Table I and treating β_2^C and β_2^N as adjustable parameters. The separate contributions from Coulomb excitation (dot-dash curve) and nuclear excitation (dotted curve) are also shown.

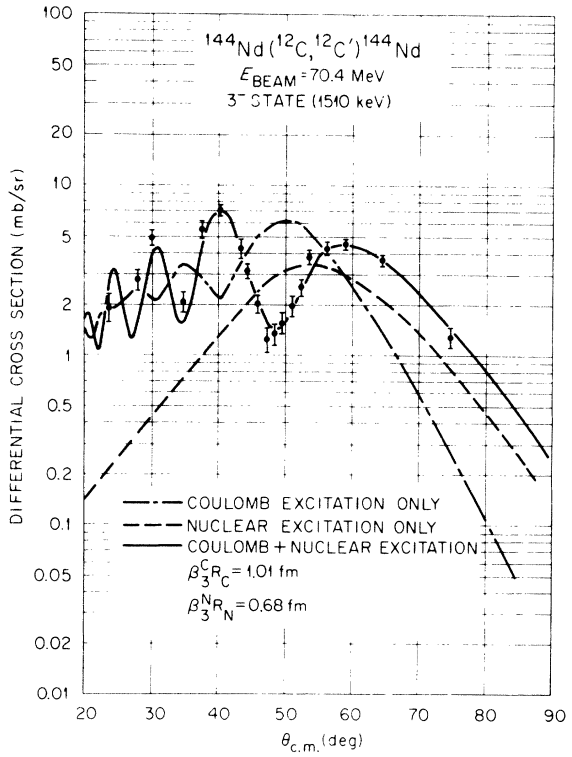

FIG. 5. Differential cross section for exciting the 3^- (1511-keV) level in ^{144}Nd by 70.4-MeV ^{12}C inelastic scattering. The solid curve is a DWBA fit to the data using the potential of Table I and treating β_3^C and β_3^N as adjustable parameters. Separate contributions from Coulomb excitation (dot-dash curve) and nuclear excitation (dotted curve) are also shown.

TABLE IV. Deformation parameters and quadrupole moment measurements taken from previous Coulomb-excitation experiments in comparison with theoretical predictions for Q_2.

			Previous Coulomb excitation					Theory	
Nucleus	E^* (keV)	J^π	$B(El)\uparrow$ (e^2b^l)	$B(El)\uparrow$ [a] (spu)	β_l^C [b]	$\beta_l^C R_C$ [b] (fm)	Q_2 (e b)	$\lvert Q_{rot}\rvert$ [c] (e b)	Q_2 [d] (e b)
142	1572	2^+	0.34 [e]	15.6	0.096	0.626	...	0.53	−0.13
	2080	3^-	0.24 [f]	28.6	0.123	0.802	...	...	...
144	696	2^+	0.40 [e]	18.0	0.102	0.668	−0.39 [g]	0.57	−0.7
	1510	3^-	0.26 [h]	30.2	0.126	0.825	...	...	...
146	454	2^+	0.76 [g]	33.5	0.140	0.991	−0.72 [g]	0.79	−0.57
	1190	3^-	0.24 [i]	27.1	0.120	0.790	...	...	...
148	310	2^+	1.36 [g]	58.9	0.186	1.230	−1.36 [g]	1.056	−0.94
	1020	3^-	...	...	...	...	...	...	...
150	130	2^+	2.65 [e]	112.7	0.257	1.707	−2.00 [g]	1.475	−1.50
	950	3^-	...	...	...	...	...	...	...
	400	4^+	...	...	0.03 [j]	0.191 [j]	...	...	...
^{12}C	4430	2^+	0.0042 [e]	5.18	0.55	1.574	...	0.06	...

[a] For $B(E2)\uparrow$, 1 spu $= 2.95\times10^{-5}A_2^{4/3}\ e^2b^2$; for $B(E3)\uparrow$, 1 spu $= 4.158\times10^{-7}A_2^2\ e^2b^3$.

[b] β_l^C deduced from Eq. (2) and assuming $R_C = 1.25A_2^{1/3}$.

[c] $\lvert Q_{rot}\rvert = (-2/7)[(16\pi/5)]^{1/2}[B(E2)\uparrow]^{1/2}$ and is the spectroscopic quadrupole moment as given by the rotational model.

[d] See Ref. 28. Quadrupole moments deduced by Rezwani *et al.* using the method of potential energy surfaces.

[e] See Ref. 22.

[f] See Ref. 23.

[g] See Ref. 11.

[h] See Ref. 25.

[i] See Ref. 24.

[j] See Ref. 27.

Analysis of the data was performed using the coupled-channels code ECIS.[26] All calculations included 200 partial waves and the integrations were carried out to 50 fm in steps of 0.085 fm.

A. Optical potentials

Optical-model parameters for use in the coupled-channels calculations were determined by searching on the elastic scattering data with 0^+-2^+ coupling included for each target nucleus. These calculations employed rotational-model form factors and the previously measured transition rates and quadrupole moments[11,22,25] shown in Table IV. For ^{142}Nd a quadrupole moment half that of ^{144}Nd was used since there was no previous measurement of this quantity. The Coulomb and nuclear deformation lengths were held equal in these searches. A more detailed description of the relations between various matrix elements and deformations will be given below. Starting with the "common real potentials" shown in Table II (but with $r' = 1.341$ fm for all cases) and searching only on W and a', the potentials shown in Table V were determined by minimizing χ^2 for each target. It is evident that inclusion of the 0^+-2^+ coupling greatly reduces the large differences in the imaginary potentials shown in Table II. In fact an "average" imaginary potential with $W = 13.7$ MeV, $a' = 0.421$ fm fits all data quite well, increasing χ^2 by only 16% for the worst case as compared with the best-fit parameters shown in Table I. Similar effects of coupling on the elastic scattering of 50-MeV α particles from Sm isotopes have been reported by Glendenning, Hendrie, and Jarvis.[18] Subsequent calculations showed that coupling to excited states other than the first 2^+ state had little effect on the elastic scattering predictions so the parameters of Table V did not have to be changed when other states were added to the calculations.

TABLE V. Imaginary well parameters resulting from a CC fit to elastic scattering in a calculation which couples the ground state and the lowest 2^+ state in the rotational model. The imaginary radius is fixed at $r' = 1.341$ and the real potential is $V = 20.0$ MeV, $r_0 = 1.315$ fm, $a_0 = 0.562$ fm, and $r_C = 1.25$ fm.

	^{142}Nd	^{144}Nd	^{146}Nd	^{148}Nd	^{150}Nd
W (MeV)	13.80	10.88	15.52	10.77	17.64
a' (fm)	0.414	0.414	0.414	0.505	0.356
σ_r (b)	1.244	1.261	1.318	1.390	1.325

B. Inelastic transitions to $2^+, 4^+, 6^+$ states

Coupled-channels calculations for low-lying even-parity states were done mostly within the framework of the axially symmetric rotational model. Coulomb deformations were deduced from the relation

$$[B(El; 0^+ \rightarrow l^\pi)]^{1/2} = \frac{3Z_2 R_c^l}{4\pi} \beta_l \qquad (2)$$

using previously determined[11,23] $B(El)$'s with $R_C = 1.25A_2^{1/3}$ fm. Nuclear quadrupole deformations were then fixed in the calculations by applying simple βR scaling, i.e.:

$$\beta_l^N R_N = \beta_l^C R_C \qquad (3)$$

with $R_N = 1.315A_2^{1/3}$ fm.

Form factors for both Coulomb and nuclear excitation were then calculated using the rotational model.[10] The β_2^N values for Nd isotopes obtained by using Eq. (3) differ from those obtained from the Hendrie procedure[1] by 1% for ^{142}Nd and 2% for ^{150}Nd.

Schematic representations of transitions included in the calculations are shown in Figs. 6(a) (^{144,146,148}Nd) and 6(b) (^{150}Nd); only 0^+-2^+ coupling calculations were performed for ^{142}Nd. The $E4$ matrix elements $\langle 0^+ \| M(E4) \| 4^+ \rangle$ were determined empirically as discussed below. Possible contributions from β_6 deformations were neglected in the final calculations.

Fortunately the quadrupole moments of the 2^+ states have been measured[11,29] for $^{144-150}$Nd using Coulomb-excitation reorientation. In these cases the experimental reorientation matrix elements $\langle 2^+ \| M(E2) \| 2^+ \rangle$ were used in the calculations. With the exception of these reorientation matrix elements, all quadrupole matrix elements were rotational-model expectations based on the measured[11,22] $B(E2)$'s. For ^{142}Nd several values were used as described below. In all cases the Coulomb and nuclear excitations were assumed to have the same relative matrix elements.

The results of the coupled-channels fits for ^{142}Nd are shown in Fig. 7. The quadrupole moment of the 2^+ state (Q_2) has not been previously measured. The fit (dashed curve) using the rotational model described above with $Q_2 = 0$ is inferior to the rotational-model calculation with $Q_2 = -0.20$ e b $= -0.38|Q_{\rm rot}|$. The nucleus ^{142}Nd, which has a closed neutron shell, is expected to have a zero or small quadrupole moment. The rotational-model calculation is therefore satisfying since the value of Q_2 required to fit the data is small.

The results for $^{144-150}$Nd are shown in Figs. 8–11 and in Table VI. The sensitivity of the 2^+ fits to reorientation contributions is illustrated for ^{144}Nd in Fig. 8. The reason for the failure of DWBA calculations to give consistent Coulomb and nuclear shape parameters is immediately apparent since even if Q_2 is relatively small (-0.39 e b), its effect on the 2^+ cross section at large angles is large ($\simeq$50%). Clearly the unrealistically small nuclear

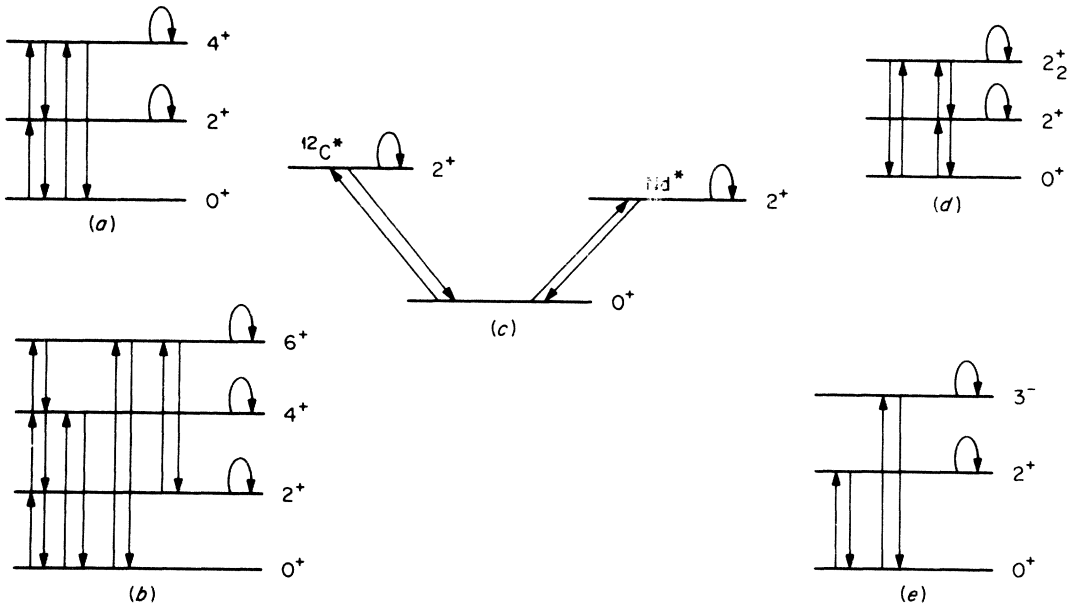

Coupling Schemes

FIG. 6. Coupling schemes investigated in the present coupled-channel analysis.

deformations shown in Table II are symptomatic of neglecting this very important contribution to the scattering.

We have performed many calculations to investigate in more detail this reorientation effect. Calculations with and without reorientation for both pure Coulomb and pure nuclear excitation reveal the somewhat surprising fact that Coulomb reorientation plays a small role in the effect even though Coulomb excitation is comparable to or stronger than nuclear excitation even at large angles (e.g., see Fig. 4). The effect is therefore mainly due to the "matter" quadrupole moment rather than to the electric quadrupole moment. This observation makes the success of the coupled-channels calculations even more satisfying—not only are β_2^C and β_2^N, which are indicative of transition strengths, consistent, but also the Coulomb and nuclear quadrupole moments, which are indicative of intrinsic shapes, are consistent.

The sensitivity of the coupled-channels calculations to the excited-state quadrupole moments suggests, of course, that this technique could be used to conveniently measure quadrupole moments of excited states. It must be noted, however, that, as in Coulomb excitation, the inclusion of other important matrix elements [such as $\langle 2^+||M(E2)||4^+\rangle$ and $\langle 0^+||M(E4)||4^+\rangle$] contributes to the excellent fits shown in Figs. 8–11 for the 2^+ states. These must be accurately known before an attempt to measure a quadrupole moment is made.

Data and coupled-channel fits for the excitation of 4^+ states are also shown in Figs. 8–11 and Table VI. These data, unlike the data for 2^+ states, could not be described successfully by the DWBA calculations regardless of the relative magnitudes of Coulomb and nuclear deformations. Furthermore, the 4^+ data display distinct nucleus-to-nucleus variations, particularly in the positions and depths of the principal interference minimum in the region of the 40–50° scattering angle. Since more than one matrix element contribute to the shape of the 4^+ angular distributions [both $\langle 0^+||M(E4)||4^+\rangle$ and $\langle 2^+||M(E2)||4^+\rangle$ are important], it would be naive to describe this minimum simply as Coulomb-nuclear interference. As can be seen in Figs. 8–11 the data are well described by assuming a rotational-model value for $\langle 2^+||M(E2)||4^+\rangle$ and treating the β_4 deformation as a free parameter (but demanding that $\beta_4^C R_C = \beta_4^N R_N$). The sensitivity to the sign and magnitude of β_4 is substantial as shown in Fig. 10.

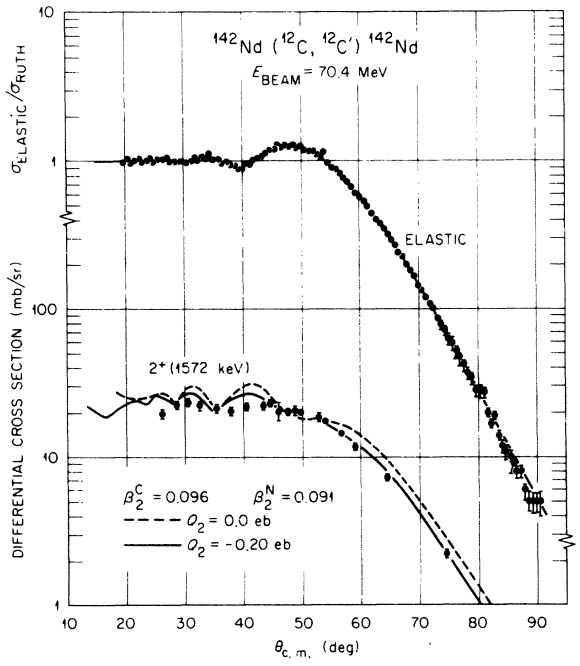

FIG. 7. Angular distributions for 70.4-MeV ^{12}C elastic and inelastic scattering from ^{142}Nd. The curves are 0^+–2^+ CC rotational-model calculations for the indicated quadrupole moments. The β_2^C deformation was obtained from the measured (Ref. 22) $B(E2)$ using Eq. (2). The potential used is from Table V.

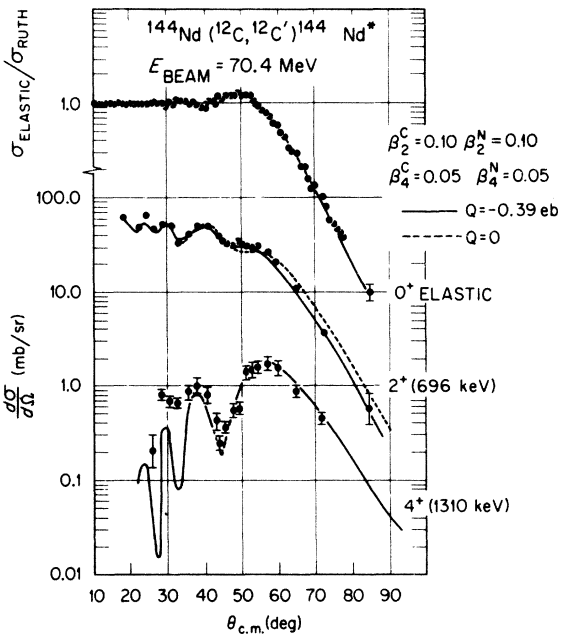

FIG. 8. Angular distributions for 70.4-MeV ^{12}C elastic and inelastic scattering from ^{144}Nd. The curves are CC rotational-model calculations using the potential of Table V and the couplings of Fig. 6(a). Coupling strengths were taken from previously published measurements (Refs. 11 and 22) except for β_4 which was adjusted to fit the observed 4^+ cross section. The sensitivity of the CC calculation to the value of Q_2 is illustrated by the dotted curve ($Q_2 = 0$) for the 2^+ state.

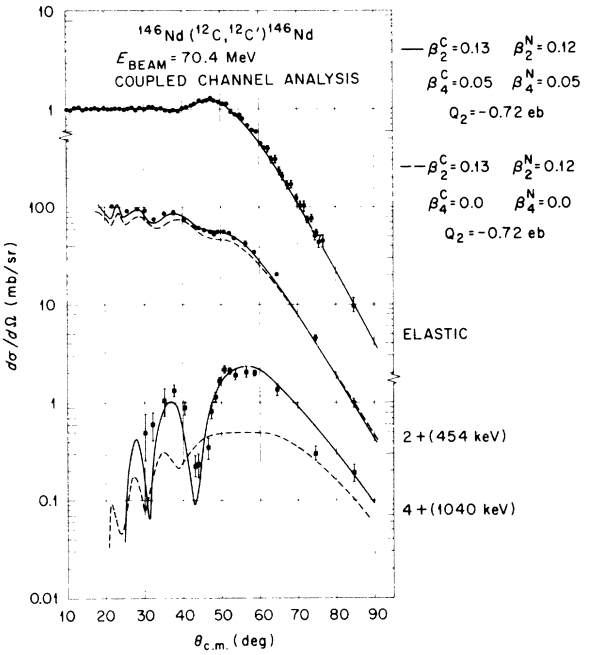

FIG. 9. Angular distributions for 70.4-MeV ^{12}C elastic and inelastic scattering from ^{146}Nd. The curves are CC rotational-model calculations using the potential of Table V and the couplings shown in Fig. 6(a). Previously reported (Ref. 11) $B(E2)$ and quadrupole moment values were used for approximate matrix elements and β_4 was allowed to vary. Sensitivity of the calculations to β_4 is shown for $\beta_4 = 0$ (dotted curve) and for $\beta_4 = 0.05$ (solid curve) which provides the best fit.

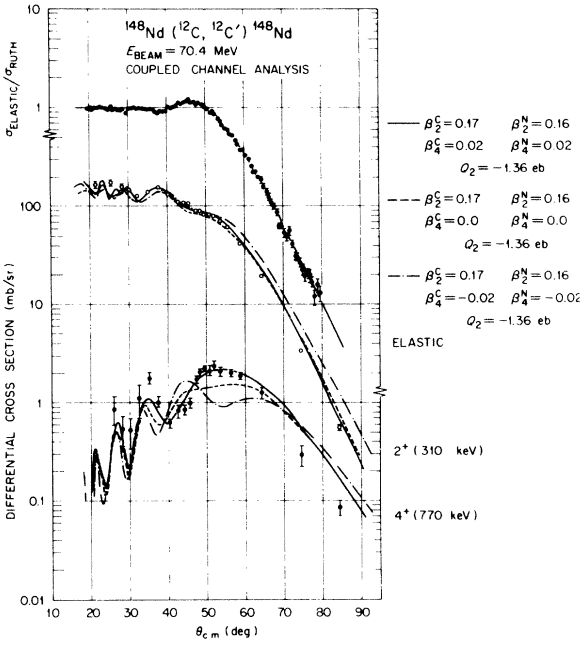

FIG. 10. Angular distributions for 70.4-MeV ^{12}C elastic and inelastic scattering from ^{148}Nd. The curves are CC rotational-model calculations using the potential of Table V and the previously reported (Ref. 11) matrix elements. The sensitivity of the analysis to the magnitude and sign of the unknown hexadecapole deformation is also illustrated.

The sensitivity to the magnitude of the matrix element $\langle 2^+||M(E2)||4^+\rangle$ is also significant as illustrated in Fig. 11; since the magnitudes of these matrix elements are not accurately known we have not attempted to deduce the reorientation matrix elements $\langle 4^+||M(E2)||4^+\rangle$ but have simply used rotational-model estimates.

A cautionary note with regard to the physical interpretation of β_4 should be made. The structure of the angular distributions results from interference between the $l=4$, $0^+ \rightarrow 4^+$ transition and the $l=2$, $0^+ \rightarrow 2^+ \rightarrow 4^+$ transition. Thus the deformation β_4 is merely a parametrization of the magnitude of $\langle 0^+||M(E4)||4^+\rangle$ and the sign of β_4 is a representation of the sign of this matrix element relative to the product $\langle 0^+||M(E2)||2^+\rangle\langle 2^+||M(E2)||4^+\rangle$. Thus the necessity of including β_4 in the calculations does not necessarily imply the existence of a permanent hexadecapole moment. However, our value of $\beta_4 = +0.03$ for ^{150}Nd is in good agreement with the Coulomb-excitation measurement of Simon *et al.*[27] ($\beta_4 = +0.03 \pm 0.02$).

The data and coupled-channels fits for the 6^+ state in ^{150}Nd are shown in Fig. 11. The quality and quantity of these data preclude a detailed analysis for this state but the data are well described without inclusion of a direct $[\langle 0^+||M(E6)||6^+\rangle]$ excitation term for this state. It is interesting to note that β_4 plays a significant role in fitting the magnitude of the cross section for the 6^+ state.

C. Inelastic transitions to 3^- states

The DWBA analysis for excitation of 3^- octupole states also leads to unrealistically large inequalities between $\beta_3^C R_C$ and $\beta_3^N R_N$ (see Table III). The prospect that these inequalities might also be removed by including reorientation transitions $[\langle 3^-||M(E2)||3^-\rangle]$ is perhaps more exciting than for the 2^+ states since Coulomb-excitation reorientation measurements of 3^- states are much more difficult due to the relatively weak Coulomb excitation for $l \neq 2$ transitions. In fact only two Coulomb-excitation reorientation measurements have been made; Barnett and Phillips[30] have reported a quadrupole moment for the 2.6-MeV level in ^{208}Pb to be -1.3 ± 0.6 eb and Joye *et al.*[31] report a value of -0.42 ± 0.32 eb for the same level.

Coupled-channels analysis of 3^- states presents a problem relative to analysis of the positive parity "ground-state band" states; octupole vibrations obviously cannot be analyzed using a simple

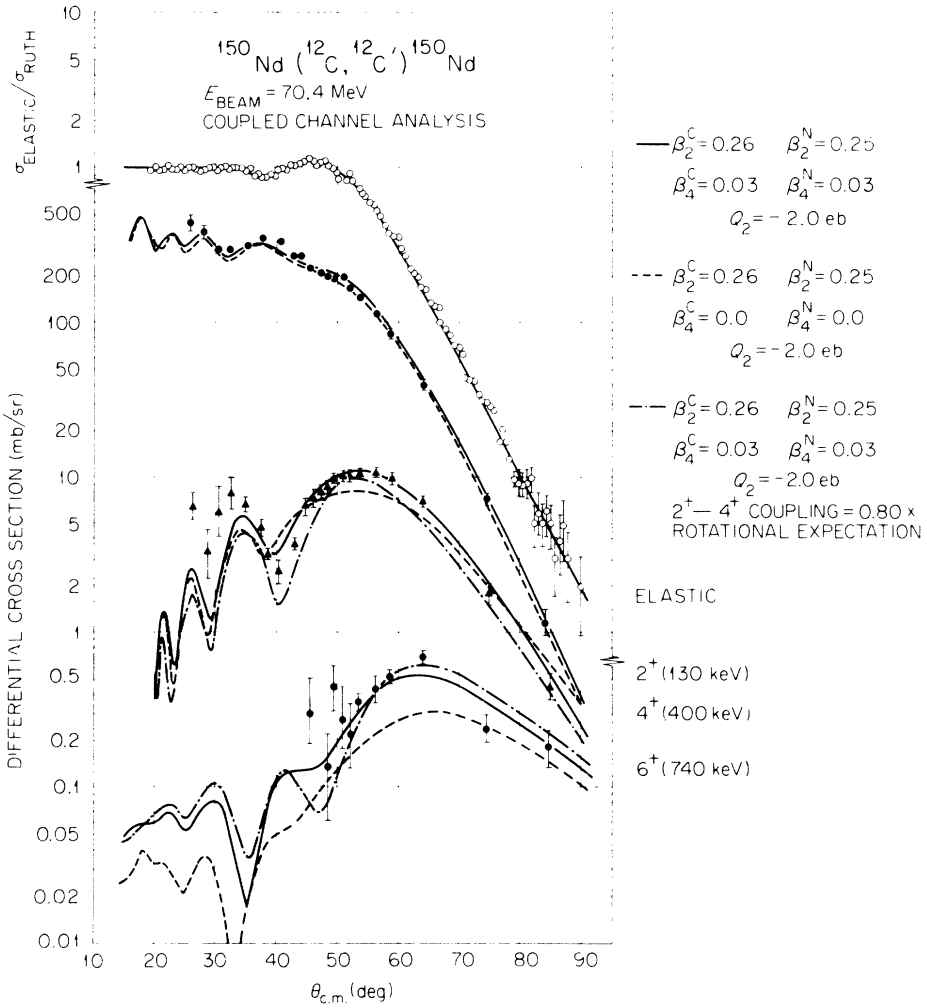

FIG. 11. Angular distributions for 70.4-MeV ^{12}C elastic and inelastic scattering from ^{150}Nd. The curves are CC rotational-model calculations using the potential of Table V and previously reported $0^+ \rightarrow 2^+$ and $2^+ \rightarrow 2^+$ matrix elements (Refs. 22 and 11). Sensitivity of the calculation to the $0^+ \rightarrow 4^+$ strength may be judged by comparing the dashed and solid curves. Sensitivity to the $2^+ \rightarrow 4^+$ matrix element is obtained by comparing the dot-dash curves with the solid curves. The calculations include the transitions shown in Fig. 6(b) with the $0^+ \rightarrow 6^+$ transition set to zero.

rotational model. The calculations were therefore done within the framework of the first-order vibrational model which is equivalent to a first-order rotational model provided that the matrix elements $\langle 2^+ \| M(E2) \| 2^+ \rangle$ and $\langle 3^- \| M(E2) \| 3^- \rangle$ are included. These matrix elements are not normally included in the first-order vibrational model, but they may be included in ECIS by input of the reduced matrix elements. The calculations were performed using the usual first-order Coulomb-excitation form factors,[20] while the nuclear excitation was determined from

$$\langle 0 \,|\, U \,|\, l^\pi \rangle = \beta_l^N R_N \frac{\delta U}{\delta r} Y_{lm} \tag{4}$$

for direct excitation and

$$\langle l^\pi \,|\, U \,|\, l^\pi \rangle = \beta_{ll}^N R_N \frac{\delta U}{\delta r} Y_{2m} \tag{5}$$

for reorientation transitions. Here, U is the complex optical potential of Table V and the value of R_N is taken to be either $R_N = r_0 A_2^{1/3}$ or $R_N = r' A_2^{1/3}$ depending on whether R_N is multiplying the real part or the imaginary part of the form factor.

The calculations included the 0^+-2^+ and 0^+-3^- couplings as shown schematically in Fig. 6(e). Previously measured[11,22,29] matrix elements $\langle 0^+ \| M(E2) \| 2^+ \rangle$ and $\langle 2^+ \| M(E2) \| 2^+ \rangle$ were used (Table IV). For $^{142-146}$Nd previously measured[23-25]

$E3$ matrix elements $\langle 0^+ \| M(E3) \| 3^- \rangle$ were used initially and then slightly readjusted to optimize the fits. For ^{148,150}Nd there are no previous measurements so $\langle 0^+ \| M(E3) \| 3^- \rangle$ was treated as a free parameter. Reorientation deformations for the 3^- states, β_{33}, were also adjusted to obtain the best fits to the data. The effects of $\langle 2^+ \| M(E3) \| 3^- \rangle$ matrix elements were found to be negligible. For all calculations $\beta_L^C R_C = \beta_L^N R_N$ and $\beta_{11}^C R_C = \beta_{11}^N R_N$ for both $L = 2$ and $L = 3$.

The results of the CC analysis for the 3^- states are shown in Fig. 12. The deformation parameters β_3 and β_{33} used in the calculations are given in Table VII and the values used for β_2 and Q_2 are those of Table VI. Sensitivity of the analysis to the 3^- reorientation matrix element is illustrated in Fig. 12 for ^{146}Nd and ^{150}Nd where the best fit (solid curves) may be compared with calculations without reorientation ($\beta_{33} = 0$, dotted curves). A distance-of-closest-approach scale (assuming Rutherford orbits) is included at the top of Fig. 12 to draw attention to the systematic change in the location of the interference minima near 50° c.m. Although there is a dramatic change in the qualitative features of the angular distributions, including the reorientation terms $\langle 3^- \| M(E2) \| 3^- \rangle$, provides excellent fits with nearly constant direct-excitation strengths for all the Nd isotopes. The 3^- reorientation deformation strength $\beta_{33}^C R_C$ increases rapidly with increasing mass of Nd much like the behavior displayed by the static quadrupole moments Q_2 in Table VI.

TABLE VI. Deformation parameters and quadrupole moments used or deduced in the coupled-channel (CC) analysis in describing the positive parity states observed for the even Nd isotopes. The quadrupole moments Q_J were used to deduce the reorientation (self-coupling) matrix elements for the 2^+ states in each of the CC calculations.

			Present analysis[a]		
Nucleus	E^* (keV)	J^π	β_I^C	$\beta_I^C R_C$ (fm)	Q_J (e b)
142	1572	2^+	0.096[b]	0.626[b]	−0.20[c]
	2380	2^+	0.023	0.150	−0.20
144	696	2^+	0.102[b]	0.668[b]	−0.39[d]
	1310	4^+	0.05[e]	0.33[e]	−0.72[f]
	2100	2^+	0.068	0.445	−0.39
146	454	2^+	0.140[b]	0.991[b]	−0.72[d]
	1040	4^+	0.05[e]	0.922[e]	−1.01[f]
	1470	2^+	0.045	0.296	−0.72
148	310	2^+	0.186[b]	1.230[b]	−1.36[d]
	770	4^+	0.015[e]	0.10[e]	−1.34[f]
	1240	2^+	0.044	0.291	−1.36
150	130	2^+	0.257[b]	1.707[b]	−2.00[d]
	400	4^+	0.03[e]	0.20[e]	−1.88[f]
	740	6^+	0.00	0.00	−2.06[f]
	1060	2^+	0.040	0.266	−2.00

[a] Throughout the CC analysis $\beta_I^C R_C = \beta_I^N R_N$, where $R_C = 1.25 A_2^{1/3}$ and $R_N = 1.315 A_2^{1/3}$.

[b] See Table IV. $\beta_2^C R_C$ and β_2^C were deduced from Eq. (2) using previously known $B(E2)\uparrow$ values.

[c] Previous measurements of Q_2 for ^{142}Nd are not available, and the value listed in this table is the value deduced from the present analysis.

[d] See Ref. 11 and/or Table IV.

[e] β_4^C is adjusted to obtain the best fit to the experimental data.

[f] The $L = 2$ reorientation matrix elements for the 4^+ and 6^+ states are given by Eq. (6), where Q_4 and Q_6 are deduced from the rotational model. $Q_4 = -0.364[16\pi/5]^{1/2} \times [B(E2)\uparrow]^{1/2}$ and $Q_6 = -0.4(16\pi/5)^{1/2}(B(E2)\uparrow)^{1/2}$.

D. Inelastic transitions to 2_2^+ states

Coupled-channels calculations for the higher-lying 2^+ states (2_2^+) were analyzed using the rotational model described in Sec. IV B above and with the couplings shown in Fig. 6(d). The matrix elements $\langle 0^+ \| M(E2) \| 2_2^+ \rangle$ and $\langle 2_2^+ \| M(E2) \| 2_2^+ \rangle$ were treated as adjustable parameters with $\beta_2^{C\prime} R_C = \beta_2^{N\prime} R_C$ where $\beta_2^{C\prime}$ is the deformation parameter deduced from $\langle 0^+ \| M(E2) \| 2_2^+ \rangle$ using Eq. (2). No reliable measurements of the "interband" transition matrix elements $[\langle 2^+ \| M(E2) \| 2_2^+ \rangle]$ have been made so these have been set equal to zero in our calculations although we recognize that they are likely to be important.

The resulting fits are shown in Fig. 13 and the deformations and quadrupole moments are listed in Table VI. The fits are generally much less impressive than for the lower 2^+ states (see Figs. 7–11). This may be due to neglecting $2^+ \rightarrow 2_2^+$ transitions, but efforts to improve the fits by including reasonable transition strengths were not successful.

Most disappointing, however, is the fact that the best fits to these data (solid curves) are for 2_2^+ quadrupole moments with signs and magnitudes equal to those for 2^+ states. The sensitivity to these quadrupole moments is illustrated for ^{150}Nd in Fig. 13. It is expected that the most strongly excited, higher-lying 2^+ states will be γ vibrations ($K = 2$), at least for the heavier Nd targets. The relationship between the spectroscopic quadrupole moment Q_{IK} with spin I and projection K on the symmetry axis and the intrinsic quadrupole moment Q_0 is

$$Q_{IK} = \frac{3K^2 - I(I+1)}{(I+1)(2I+3)} Q_0 . \tag{6}$$

One expects [see Eq. (6)] these 2_2^+ states to have quadrupole moments equal in magnitude to but of opposite sign from the 2^+ quadrupole moments. It seems unlikely that the 2_2^+ states observed are K

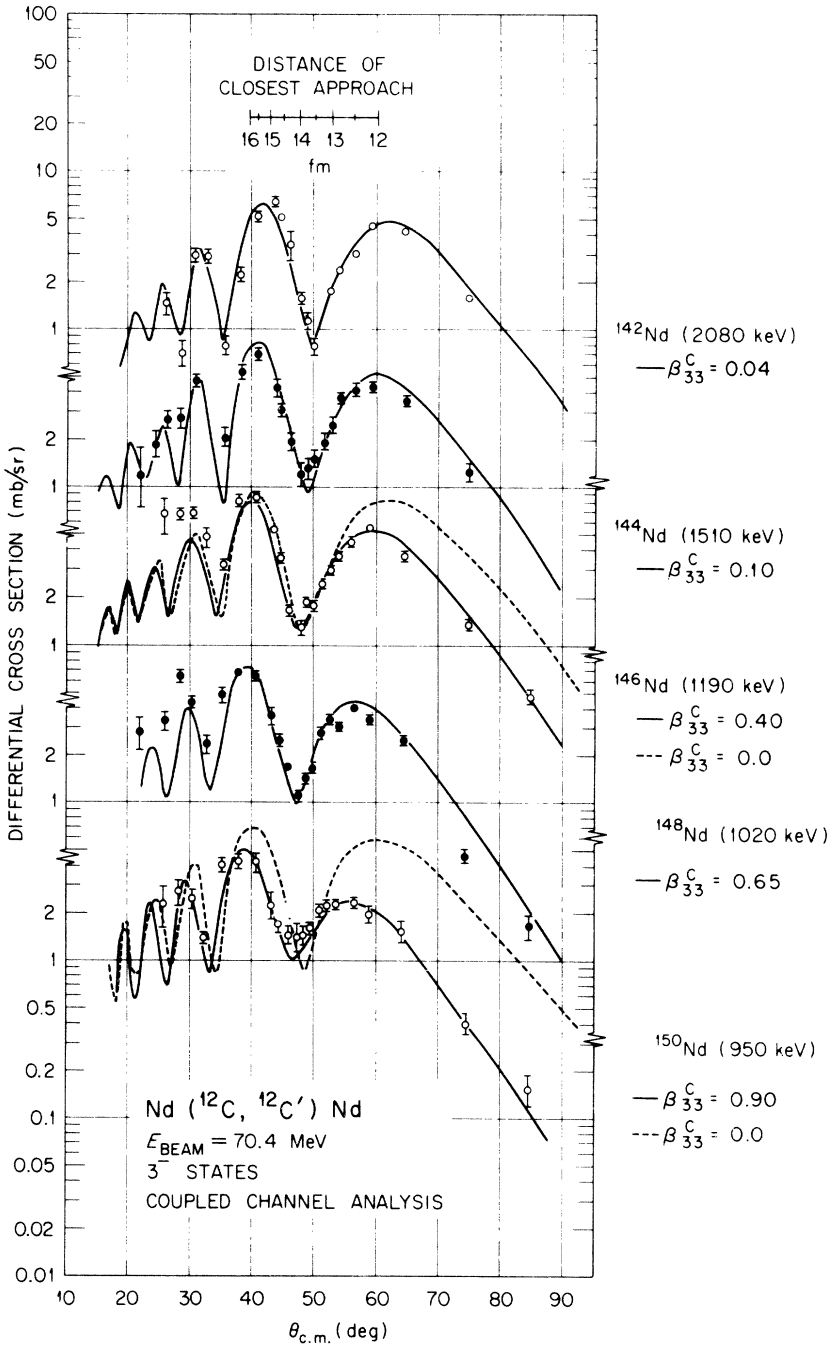

FIG. 12. Differential cross sections for exciting the 3$^-$ states of even Nd isotopes by 70.4-MeV ^{12}C inelastic scattering. The solid curves are CC first-order vibrational-model calculations using the potentials of Table V and including the couplings shown in Fig. 6(e). Where available, β_3^C values were obtained from previously measured $B(E3)$ values (Refs. 23 and 25). Reorientation deformations [see Eq. (5)] for the solid curves were adjusted to fit the data. The values used in the CC calculations for β_3 and β_{33} are listed in Table VII. Sensitivity of the analysis to the reorientation matrix elements may be judged by comparing solid and dashed curves ($\beta_{33}=0$).

= 0 states as seemingly implied by our analyses, particularly for ^{150}Nd where the 2^+ member of the β band ($K=0$) is known to lie at 840 keV (not the state we observed).

This problem cannot be fully resolved until more is known about competing mechanisms for excitations of the 2_2^+ states. It would be interesting to perform a similar experiment on a target where a more complete set of pertinent matrix elements $[\langle J^\tau \| M(E2) \| 2_2^+ \rangle]$ has been determined experimentally.

E. ^{12}C projectile excitation

Excitation of ^{12}C to the 4.43-MeV, 2^+ state appears as a Doppler broadened peak in the spectra of Fig. 1. The yield for this state was extracted by assuming a smooth continuum to underlie the peak. Within the uncertainties of this procedure, we were unable to distinguish clear differences in the differential cross sections from the various Nd isotopes. Therefore, in Fig. 14 we show a composite differential cross section for exciting the 4.43-MeV state of ^{12}C obtained by averaging data from all the Nd targets. Although the errors are large, a clear interference structure is apparent.

In the treatment of geometry, the CC program ECIS[26] makes a distinction between target and projectile. Because geometry factors appear in the potential as well as in the matrix elements, it is not a simple matter to mock up projectile excitation as a fictitious state in the target. To avoid this complication, the calculations were performed by interchanging beam and target. To obtain an estimate of β_2^C for ^{12}C from the reported[22] $B(E2)$ we used the relation:

$$[B(E2)]^{1/2} = \frac{3Z_2 e R_C^{\,2}}{5} \int (1+\beta_2^C Y_{20})^5 d\Omega \Big/ \int (1+\beta_2^C Y_{20})^3 d\Omega \qquad (7)$$

rather than Eq. (2) [which involves only the first-

TABLE VII. Deformation parameters for the 3^- states of the even Nd isotopes. Throughout the CC analysis $\beta_I^C R_C = \beta_I^N R_N$ and $\beta_{II}^C R_C = \beta_{II}^N R_N$ with $R_C = 1.25A_2^{1/3}$ and $R_N = 1.315A_2^{1/3}$.

Nucleus	E^* (keV)	Direct excitation β_3^C	Direct excitation $\beta_3^C R_C$ (fm)	Reorientation[a] β_{33}^C	Reorientation[a] $\beta_{33}^C R_C$ (fm)
142	2080	0.13[b]	0.85[b]	0.04	0.26
144	1510	0.13[b]	0.85[b]	0.10	0.66
146	1190	0.14[b]	0.92[b]	0.40	2.63
148	1020	0.14[c]	0.93[c]	0.65	4.30
150	950	0.12[c]	0.80[c]	0.90	5.98

[a] Previous reorientation matrix elements were not available; therefore β_{33} was adjusted to fit the large angle 3^- data.

[b] The values $\beta_3^C R_C$ and β_3^C were deduced from Eq. (2) using previously known $B(E3)\uparrow$ values (Table IV) and were adjusted slightly to fit the magnitude of the cross section at small angles.

[c] Previous Coulomb-excitation values were not available; therefore β_3 was adjusted to fit small angle 3^- data.

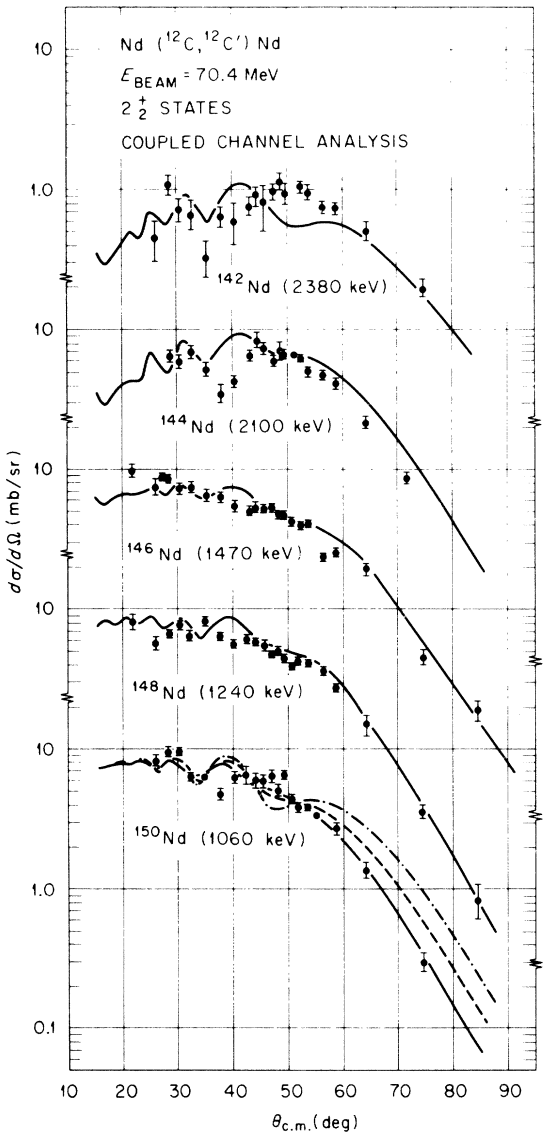

FIG. 13. Differential cross sections for exciting the 2_2^+ states of the even Nd isotopes by 70.4-MeV ^{12}C inelastic scattering. The curves are CC rotational-model calculations using the potentials of Table V and including the couplings shown in Fig. 6(d) but without the $2^+ \longleftrightarrow 2_2^+$ transition. The solid curves use deformation parameters and quadrupole moments given in Table VI. The dashed and dot-dash curves for ^{150}Nd illustrate the sensitivity of the calculation to $Q_{2_2^+}$. For the dashed curve $Q_{2_2^+} = 0.0$ and for the dot-dash curve $Q_{2_2^+} = +2.0$ *e* b.

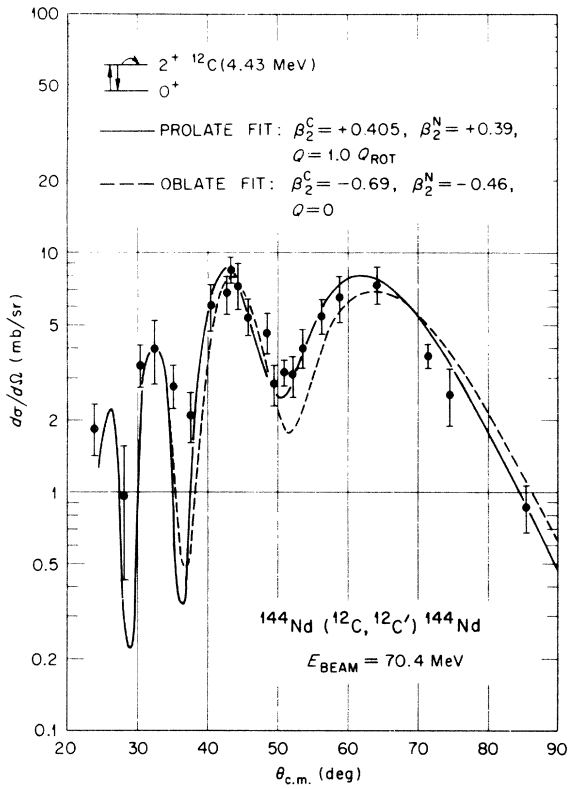

FIG. 14. Composite differential cross section for exciting the 4.43-MeV state of the 70.4-MeV ^{12}C projectile by scattering from even Nd isotopes. The curves are $0^+ \rightarrow 2^+$ CC calculations in which the nuclear potentials β_2^C, β_2^N, and Q_2 were varied to obtain the best simultaneous fit to 0^+ and 2^+ data. Prolate ($\beta_2 > 0$, solid curve) and oblate ($\beta_2 < 0$, dashed curve) calculations are compared.

order term of Eq. (7)]. With $r_C = 1.25$ fm, $B(E2) = (0.0042 \pm 0.0006)\ e^2 b^2$ in Eq. (7) we derive $\beta_2^C = -0.69 \pm 0.04$ for an oblate shape and $\beta_2^C = +0.47 \pm 0.03$ for a prolate shape. Starting with these values of β_2^C, we attempted to fit the 0^+ elastic scattering data of Fig. 2 (for ^{144}Nd) and the 2^+ data of Fig. 14 with a 0^+-2^+ rotational-model calculation. In searching for a fit to the ^{12}C 2^+ data, β_2^C was adjusted to fit the magnitude of the forward angle data, especially the maximum near 43°. Assuming a value for Q_2, we adjusted β_2^N to fit the back angle data, especially the maximum near 63°. The magnitude of Q_2 had the most influence on the location of the minimum near 50°. The potential found to provide an excellent fit to the ^{144}Nd elastic scattering data under those conditions was $V = 20.0$ MeV, $r_0 = 1.314$ fm, $a_0 = 0.51$ fm, $W = 7.0$ MeV, $r' = 1.341$ fm, and $a' = 0.414$ fm. This potential, in contrast to the potential in Table V, accounts for the influence of the low-lying 2^+ state in ^{144}Nd on the elastic scattering so that the $0^+ \rightleftharpoons 2^+$ coupling to Nd in Fig. 6(c) need not be treated explicitly in the calculation. The best fit to the ^{12}C 2^+ data, assuming an oblate shape ($\beta_2^C < 0$), is shown as a dotted curve in Fig. 14. The magnitude of β_2^C (−0.69) agrees with the reported[22] $B(E2)$. However, the value of β_2^N is considerably smaller than expected from βR scaling and the location of the primary interference minimum is misplaced by almost 2°. If the value of $|Q_2|$ is increased from 0, the mismatch in phase becomes worse. The best fit for a prolate shape ($\beta_2^C > 0$) is shown as the solid curve in Fig. 14. This fit appears satisfactory, although the value of β_2^C (+0.405) is somewhat lower than expected from the reported[22] $B(E2)$, but the value of β_2^N is consistent with βR scaling. The value $Q_2 = 1.0 Q_{rot}$ gives the best representation of the phase. The fact that the data are best fitted by a prolate shape is surprising since ^{12}C is expected to be strongly oblate in its first 2^+ state. Contrary to the conclusion reported in our previous analysis,[8] we cannot claim definitive evidence for an oblate shape of ^{12}C in its 4.43-MeV state. Additional experimental and theoretical studies of projectile excitation would be useful.

VI. SUMMARY AND CONCLUSIONS

Using the coupled-channels approach, we have shown that heavy-ion inelastic scattering at energies above the Coulomb barrier involves a variety of multistep processes. We have successfully accounted for the influence of these processes on elastic scattering with a consistent nuclear potential for all Nd isotopes. In combination with previous Coulomb-excitation measurements, we were able to extract new information on hexadecapole deformations and to demonstrate a particular sensitivity to the nuclear reorientation effect. We conclude that these kind of data and analyses can provide a rich source of information on collective nuclear structure.

ACKNOWLEDGMENTS

We are indebted to J. L. C. Ford for his contributions towards development of the focal plane detector. D. Martin and T. Slamon were very helpful in the data reduction stages. It is a pleasure to acknowledge helpful discussions on coupled-channels analysis with L. D. Rickertsen, R. Ronningen, and C. E. Bemis. Finally, M. B. Marshall and the operations staff are to be congratulated for flawless operation of the ORIC cyclotron.

*Oak Ridge Graduate Fellow from the University of Tennessee. Present address: Niels Bohr Institute, Copenhagen, Denmark.

†Work supported by Union Carbide Corp. under contract with the U.S.E.R.D.A.

‡Supported in part by the U.S.E.R.D.A.

§Work supported by NSF grant No. PHY 76-08788 and Oak Ridge Associated Universities, Inc.

[1]D. L. Hendrie, Phys. Rev. Lett. 31, 478 (1973).

[2]F. Videbaek, I. Chernov, P. R. Christensen, and E. E. Gross, Phys. Rev. Lett. 28, 1072 (1972).

[3]F. D. Becchetti, D. G. Kovar, B. G. Harvey, J. Mahoney, B. Moyer, and F. G. Pühlhofer, Phys. Rev. C 6, 2215 (1972).

[4]P. R. Christensen, I. Chernov, E. E. Gross, R. Stokstad, and F. Videbaek, Nucl. Phys. A207, 433 (1973).

[5]J. L. C. Ford, K. S. Toth, D. C. Hensley, R. M. Gaedke, P. J. Riley, and S. T. Thornton, Phys. Rev. C 8, 1912 (1973).

[6]E. E. Gross, H. G. Bingham, M. L. Halbert, D. C. Hensley, and M. J. Saltmarsh, Phys. Rev. C 10, 45 (1974).

[7]F. Videbaek, P. R. Christensen, O. Hansen, and K. Ulbak, Nucl. Phys. A256, 301 (1976).

[8]D. L. Hillis, E. E. Gross, D. C. Hensley, L. D. Rickertsen, C. R. Bingham, A. Scott, and F. T. Baker, Phys. Rev. Lett. 36, 304 (1976).

[9]J. X. Saladin, I. Y. Lee, R. C. Haight, and D. Vitous, Phys. Rev. C 14, 992 (1976).

[10]T. Tamura, Rev. Mod. Phys. 37, 679 (1965).

[11]P. A. Crowley, J. R. Kerns, and J. X. Saladin, Phys. Rev. C 3, 2049 (1971).

[12]E. E. Gross, Nucl. Instrum. Methods 135, 401 (1976).

[13]J. B. Ball, C. B. Fulmer, E. E. Gross, M. L. Halbert, D. C. Hensley, C. A. Ludemann, M. J. Saltmarsh, and G. R. Satchler, Nucl. Phys. A252, 208 (1975).

[14]E. E. Gross, Nucl. Instrum. Methods 121, 297 (1974).

[15]C. J. Borkowski and M. K. Kopp, Rev. Sci. Instrum. 39, 1515 (1968); IEEE Trans. Nucl. Sci. NS-17, 340 (1970).

[16]J. L. C. Ford, K. S. Toth, G. R. Satchler, D. C. Hensley, L. W. Owen, R. M. DeVries, R. M. Gaedke, P. J. Riley, and S. T. Thornton, Phys. Rev. C 10, 1429 (1974).

[17]J. G. van der Baan, P. R. Christensen, J. Rasmussen, and P. O. Tjøm, Nucl. Phys. A115, 265 (1968).

[18]N. K. Glendenning, D. L. Hendrie, and O. N. Jarvis, Phys. Lett. 26B, 131 (1968).

[19]F. G. Perey (private communication).

[20]R. H. Bassel, G. R. Satchler, R. M. Drisko, and E. Rost, Phys. Rev. 128, 2693 (1962).

[21]P. D. Kunz (private communication).

[22]P. H. Stelson and L. Grodzins, Nucl. Data A1, 1 (1965).

[23]D. W. Madsen, L. S. Cardman, J. R. Legg, and C. K. Bockelman, Nucl. Phys. A168, 97 (1971).

[24]Nuclear Data Sheets 14, 444 (1975).

[25]O. Hansen and O. Nathan, Nucl. Phys. 42, 197 (1963).

[26]J. Raynal (private communication).

[27]R. S. Simon, J. de Boer, G. Dannhäusser, R. J. Lutter, F. Riess, and H. Steffens, in *Proceedings of the International Conference on Nuclear Physics, Munich, 1973*, edited by J. de Boer and H. J. Mang (North-Holland, Amsterdam/American Elsevier, New York, 1973), p. 292.

[28]V. Rezwani, M. Brand, R. Sedlmayr, L. V. Berus, U. Schneider, and W. Greiner, in *Proceedings of the International Conference on Nuclear Structure Studies Using Electron Scattering and Photoreactions, Sendai, Japan, 1972*, edited by K. Shoda and H. Ui (Tohoku Univ., Sendai, Japan, 1972), Supplement to Research Report of Laboratory of Nuclear Science, Tohoku University, Vol. 5, p. 235.

[29]H. S. Gertzman, D. Cline, H. E. Gove, and P. M. S. Lesser, Nucl. Phys. A151, 282 (1971).

[30]A. R. Barnett and W. R. Phillips, Phys. Rev. 186, 1205 (1969). Revised values appear in D. H. Feng, A. R. Barnett, and L. J. B. Goldfarb, Phys. Rev. C 13, 1151 (1976).

[31]A. M. R. Joye, A. M. Baxter, M. P. Fewell, D. C. Kean, and R. H. Spear, Phys. Rev. Lett. 38, 807 (1977).